RESEARCH

Electron paramagnetic resonance signature of rock-forming blue quartz from the Albești (Romania) granite

Alexandra C. Joita[1] · Daniela Ghica[1] · Mariana Stefan[1] · Stefan Bulat[1] · Adrian I. Pantia[2,3]

Abstract

The ca. 480 Ma Albești granite (Southern Carpathians, Romania) is characterized by the presence of color zoned blue quartz grains, and is part of the rather extensive European Cambro-Ordovician blue quartz landscape. The color is heat sensitive, fading at temperatures as low as 300°C, inconsistent with the thermally stable, light scattering, nanometric rutile/ilmenite inclusions cited in literature. Extensive X- and Q-band electron paramagnetic resonance (EPR) investigations were carried out, searching for distinctive features of the Albești quartz that are directly or indirectly involved in the generation of the blue coloration. The analyzed quartz grains were extracted from three granite samples of varying coloration and anisotropy, and the quartz from each rock sample was further separated into colored and colorless fractions. The paramagnetic E' and $[AlO_4]^0$ centers, as well as Mn^{2+} ions localized in traces of amorphous associated minerals at grain boundaries or fissure planes, were observed in all quartz samples. Broad EPR lines associated with the presence of magnetic clusters were observed in the spectra of the white quartz sample and the corresponding colorless one. Isochronal annealing up to 500°C induced the correlated recombination of the E' and $[AlO_4]^0$ centers, the strong decrease of the Mn^{2+} spectrum and the formation of a minority iron oxide phase at the grain boundaries and/or fissure planes. The EPR signature was similar for the colored and the corresponding colorless quartz samples, before and after annealing, showing that the heat sensitive coloration of the Albești quartz does not directly involve the presence of paramagnetic defects and/or minority magnetic phases.

All authors contributed equally to this work.

Editorial handling: L. Nasdala.

✉ Mariana Stefan
  mstefan@infim.ro

✉ Adrian I. Pantia
  padrian.iulian2020@gmail.com

[1] National Institute of Materials Physics, Atomistilor 405A, Magurele 077125, Romania

[2] Geological Institute of Romania, Caransebes 1, Bucharest 012271, Romania

[3] Romanian Academy, Calea Victoriei 125, Bucharest 010071, Romania

Introduction

Ever since the pioneering work of Iddings (1904) in the Llano area (Texas, USA), the color of rock-forming blue quartz has been attributed, more often than not, to the scattering of light by submicron mineral inclusions. Indeed, Zolensky et al. (1988) concluded, in what was to become a paper of reference on the topic that the blue color of the quartz from the Llano rhyolite (llanite) is owed to light scattering rounded ilmenite ($FeTiO_3$) inclusions, ca. 60 nm across. The current understanding of blue quartz can be summed up as follows: nanometer size mineral inclusions, usually rutile (TiO_2) or ilmenite, scatter light according to the Rayleigh model. The finer points of this explanation are still disputed. Rayleigh scattering is strongly dependent on the size of the scattering centers, and yet the literature on blue quartz reports scattering inclusions ranging from 27 nm (Seifert et al. 2011) up to 300 nm (Nassau 1983), and neither the difference between the refractive index of the inclusion and the host quartz, nor

the geometry of the inclusions are considered. There are in excess of 500 rock-forming blue quartz occurrences worldwide, and the vast majority was not specifically investigated in terms of the cause of their color. Of these, 6 are located in Romania, with another 7 yet to be confirmed in the field. Their age and location likely connect them to magmatic events associated with the opening and abortion of the eastern branch of the Rheic Ocean, a feature shared with a host of other European occurrences spanning from Spain to the Czech Republic, and hint at a set of unidentified regional scale geological/geochemical conditions which enabled the manifestation of the blue color in primary quartz. Similar large scale correlations are observed in the case of the Grenville and Pan-African orogenic belts, where the nature and geological significance of this mineralogical phenomenon are equally unclear.

It is safe to assume that the current understanding may not be universally applicable, at best. A telling example is the blue quartz from the Rumburk granite (Germany): Seifert et al. (2009) identified submicron size rutile needles which were reported as the scattering centers responsible for the blue color; Seifert et al. (2010) have not identified rutile needles in different samples of blue quartz from the Rumburk granite; Seifert et al. (2011) report rutile inclusions once more. This example points to the fact that rutile, or mineral inclusions in general, may not always be a necessary condition for the blue color in quartz, and that there are other causes as well. Not all blue quartz is the same.

Several other causes for the blue color have been suggested, based on the presence of isolated impurities rather than mineral inclusions: Eu^{2+} and Ce^{3+} activator ions (Kim et al. 2015), lattice bound Ti (Pelletier 2016), Fe^{2+} in interstitial sites (Rossman 1994) or Co^{2+} (Rossman 1994; Götze et al. 2021). Other authors note an association between strain and the blue coloration of quartz, but in the absence of dedicated studies, it is unclear whether the strain merely facilitates the formation of light scattering inclusions, or the lattice distortions themselves scatter light or modify the absorption spectrum of quartz.

The 481.16 ± 10.83 Ma (Negulescu 2013) Albești granite is located in the Leaota Metamorphic Suite, Iezer Complex, Southern Carpathians, Romania. The most striking macroscopic feature of the granite is the blue color of the quartz crystals (Fig. 1a), which varies from slightly blue (even whitish) to sky blue. The quartz grains often show clear, colorless cores surrounded by a band of blue color (Fig. 1b), which is sometimes visible with the naked eye. The colored portions of the grains always present a milky appearance, a typical feature of colloidal, light scattering, mediums, which is absent in the colorless areas.

Based on Pantia and Filiuță (2021) and, as of yet, unpublished transmission electron microscopy (TEM) results, the blue quartz from the Albești granite is not characterized by inclusions small enough (Nassau 1983) to preferentially scatter blue light (although they are scarcely present). As noted by Pantia and Filiuță (2021) there is an inverse correlation between the intensity of the blue color and the degree of deformation of both the host rock and quartz, a feature shared with other blue quartz occurrences. The same study also reports a progressive loss of color during heating, culminating with complete whitening at 600℃. This points to temperature sensitive scattering centers, and dismisses the rutile or ilmenite, as the later are stable at said temperatures. The Llano blue quartz, on the other hand, maintains its color even when heated to 1000℃. Buhay et al. (1988) suggest that deformation and temperature can reset the EPR signals in quartz and, when coupled with the observations of Pantia and Filiuță (2021), a solid argument for investigating a possible connection between paramagnetic centers and color and color intensity emerges.

EPR is often used to detect low concentrations of paramagnetic point defects (intrinsic, radiation induced or impurity related) (Ghica et al. 2014), as well as minority phases difficult to observe by structural methods such as X-ray diffraction (XRD) or TEM because of their very low concentrations (< 2 wt%), non-uniform distribution and/or high degree of structural disorder (Nistor et al. 2016; Mihalcea et al. 2024). Both natural and artificial quartz have been thoroughly investigated using EPR, and the works of Perlson

Fig. 1 The Albești granite. (**a**) general appearance; (**b**) polished blue quartz grain showing color zoning
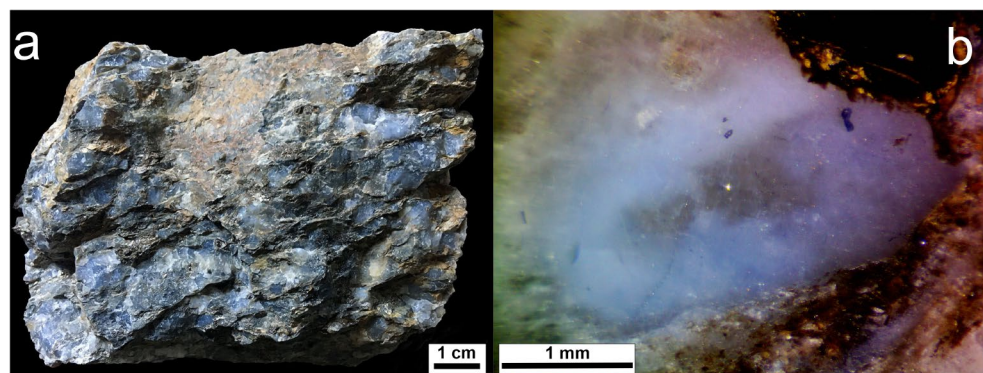
and Weil (2008), Götze (2009), Preusser et al. (2009), Mashkovtsev and Pan (2013) and Götze et al. (2021) summarize a rather comprehensive picture of the topic. The correlation between paramagnetic centers and cathodoluminescence emission bands is well known, but the literature on the paramagnetic properties of the colored varieties of quartz is virtually nonexistent. The EPR investigations performed on blue quartz from basement metasedimentary rocks the Arrow uranium deposit (Athabasca Basin, Saskatchewan, Canada) have shown a low concentration of radiation induced defects, even lower than in the case of milky or clear quartz (Cerin et al. 2017). However, Cerin et al. (2017) merely touches on the subject of blue quartz, as the paper is not dedicated to the topic.

This work is focused on the identification and characterization of the paramagnetic centers present in the Albești quartz, in search for distinctive features that could be directly or indirectly involved in the generation of the characteristic heat sensitive blue coloration. The determination of the EPR signature is one of the first steps in an ongoing investigation by various methods that will serve to further the knowledge about the Albești quartz in particular, and blue quartz in general, and provide a thorough picture that will help to determine the blue coloration mechanism.

Materials and methods

Sample preparation

Three granite samples, collected from the area of the Dragoslavele village, Argeș County, Romania, were selected based on the overall chromatic appearance and anisotropy, as follows: an isotropic sample, with sky blue, milky quartz grains, marked Q1, a slightly anisotropic sample, with pale blue, milky quartz grains (Q2), and a strongly anisotropic sample, with rusty-weathered biotite, containing white, milky quartz (Q3). All three samples contained both blue/white and colorless, clear quartz domains, in large enough quantities to allow for a highly selective separation by chromatic and purity criteria. The samples were crushed and sieved, and the grains were manually sorted under the binocular microscope into three main categories: quartz, feldspar (albite) (Ab) and biotite (Bt), representing the main constituent minerals of the Albești granite. As seen under the petrographic microscope, sericite is expected in association with the feldspar grains, and chlorite and epitaxial rutile, as well as some zircon and monazite are likely to accompany some of the sorted biotite.

The quartz grains from each sample were further separated into colorless, marked "-", and white (Q3) or blue (Q1 and Q2) colored, marked "+", eliminating the grains which were too thin to accurately assess. The separation was initially performed against a black, mate, background, and the separated grains were verified against a white background, to ensure that the grains are as free as optically discernible from mineral inclusions. The resulting quartz batches, as well as the feldspar and biotite fractions, were manually ground into a fine powder in an agate mortar.

The powder samples were inserted in calibrated pure fused-silica tubes with 2 mm and 3 mm inner diameter for the Q- and X-band EPR experiments, respectively. Annealing treatments in air were performed in steps of 100°C up to 500°C, by inserting the EPR tubes containing the samples in a temperature stabilized (± 1°C) furnace and keeping them for 30 min at the set temperature.

X-ray diffraction

The XRD investigations were carried out on manually selected quartz, feldspar and biotite fractions from Q2, which were ground into a fine powder and measured using a Bruker D8 Advance powder diffractometer with a vertical goniometer, θ-2θ configuration, and Cu anode ($\lambda = 1.5406$ Å) over a 4–90° 2θ interval. The results were interpreted using the Diffrac + Basic (Eva 13) dedicated software.

Electron paramagnetic resonance spectroscopy

Q-band (34 GHz) EPR investigations were carried out at room temperature (RT) and 90 K on an ELEXSYS E500 Bruker spectrometer equipped with an ER5106QT-W Q-band probehead and an ER4112HV-Q/FT Helium temperature system. X-band (9.8 GHz) EPR spectra were recorded at RT using an ELEXSYS E580 Bruker spectrometer equipped with an ER4118X-MD5 X-band dielectric resonator. The magnetic field at the sample was calibrated using a BDPA (alpha, gamma–bisdiphenylene-beta-phenyl allyl) reference sample, with an EPR line centered at g = 2.00276. The determination of the spin Hamiltonian parameters and the lineshape simulation of the EPR spectra were performed with the EasySpin v. 5.2.35 software (Stoll and Schweiger 2006).

Results

The optical observations of the quartz grains from the Albești granite have revealed that they are blue in reflected light and brownish-yellow in transmission. This color variation is characteristic of scattering mediums, and consistent with the literature on blue quartz. However, the identity of the scattering centers has not been determined with a reasonable degree of certainty. The optical petrographic microscopy,

as well as scanning electron microscopy (SEM) and TEM investigations (to be published later) revealed the presence of scarce rutile and ilmenite inclusions in the micro- to nanometer range which, although somewhat consistent with the literature on the subject, are not readily identifiable as the cause of the blue color, as exemplified by the case of the blue quartz from the Rumburk granite.

The XRD patterns recorded on the quartz, biotite and feldspar fractions separated from the Q2 granite are displayed in Fig. S1 in the electronic supplementary material (ESM). The X-ray diffraction patterns evidenced the presence of only quartz and biotite in the first two samples, respectively, while in the feldspar fraction albite and muscovite were identified.

The EPR spectra of all quartz and associated mineral samples were recorded at RT in both Q- and X-band (Fig. 2). The spectra of the three pairs of associated mineral Ab and Bt samples extracted from the three different granite rocks were very similar and, therefore, only one set of them was further used as reference.

Figure 2a displays the Q-band EPR spectra recorded at RT and 3.2 mW microwave power. All quartz spectra display a set of six lines with similar amplitude, linewidth and separation (~ 9.4 mT), centered at ~ 1218 mT ($g \sim 2.0$), associated with the presence of isolated Mn^{2+} ions (Miyako and Date 1964; Rao et al. 1989). Narrower lines with different saturation properties can also be observed in the quartz spectra, situated close to the center of the Mn^{2+} spectrum. As further shown, they belong to E'-type centers associated with oxygen vacancies.

Strong lines characteristic to isolated Mn^{2+} ions are present in both Q- and X-band spectra of the associated minerals as well. In the case of the biotite sample, the X-band spectrum exhibits an eight lines hyperfine structure, characteristic to vanadyl VO^{2+} ions. The VO^{2+} spectrum can be described reasonably well with the parameter values $g_x = g_y = 1.97$, $g_z = 1.943$ and $A_x = A_y = 6.0$ mT, $A_z = 18.0$ mT (Fig. S2 in ESM). The Ab and Bt X-band spectra (Fig. 2b) also contain intense lines characteristic to isolated Fe^{3+} ions in sites with rhombic ($g \sim 4.2$) and axial ($g \sim 6$) symmetry (Nicolini et al. 2009). Some of the quartz X-band spectra (Q2+, Q2-) exhibit very weak lines in the same positions, most likely due to traces of the associated minerals. The narrow signal at ~ 180 mT present in all X-band spectra belongs to the resonator. The Q- and X-band spectra of the Q3 + and Q3- quartz samples show broad lines that are not present in the spectra of the associated minerals.

Thus, the Q-band spectra of the Q3 + and Q3- samples at RT (Figs. 2a and 3a) exhibit broad (peak to peak linewidth $\Delta B \sim 110$ mT and $\Delta B \sim 54$ mT, respectively), intense lines at ~ 1100 mT ($g_{eff} \sim 2.21$) and ~ 1030 mT ($g_{eff} \sim 2.37$), respectively. As shown in Fig. 3a, at 90 K the broad line from the Q3 + spectrum moves to a lower field ($g_{eff} \sim 2.44$) and broadens further to $\Delta B \sim 170$ mT, while the broad line from the Q3- spectrum is not observable anymore. This behavior is characteristic to magnetically ordered phases (Mihalcea et al. 2024) present as either magnetic clusters in quartz or small grains from the surrounding minerals. However, as none of these signals appears in the associated mineral spectra (Fig. 3b), the first assignment is more likely. In the case of the associated mineral samples, the broad lines at ~ 1200

Fig. 2 (**a**) Q - and (**b**) X - band EPR spectra measured at RT on the six quartz samples (black), together with the background spectrum measured with empty silica tubes (green) and associated mineral Ab (red) and Bt (blue) spectra
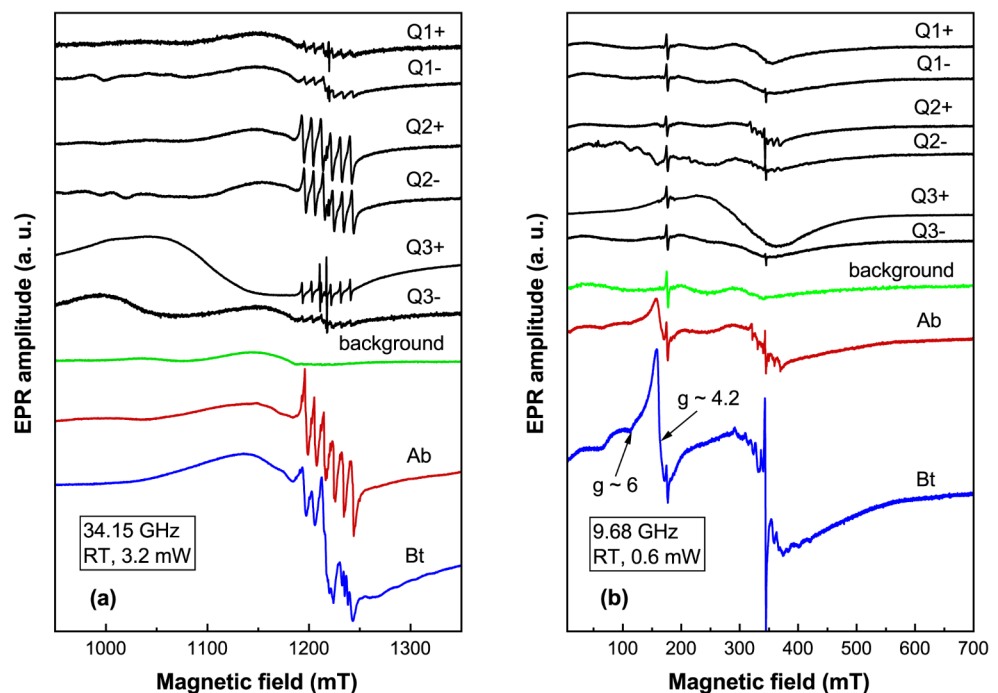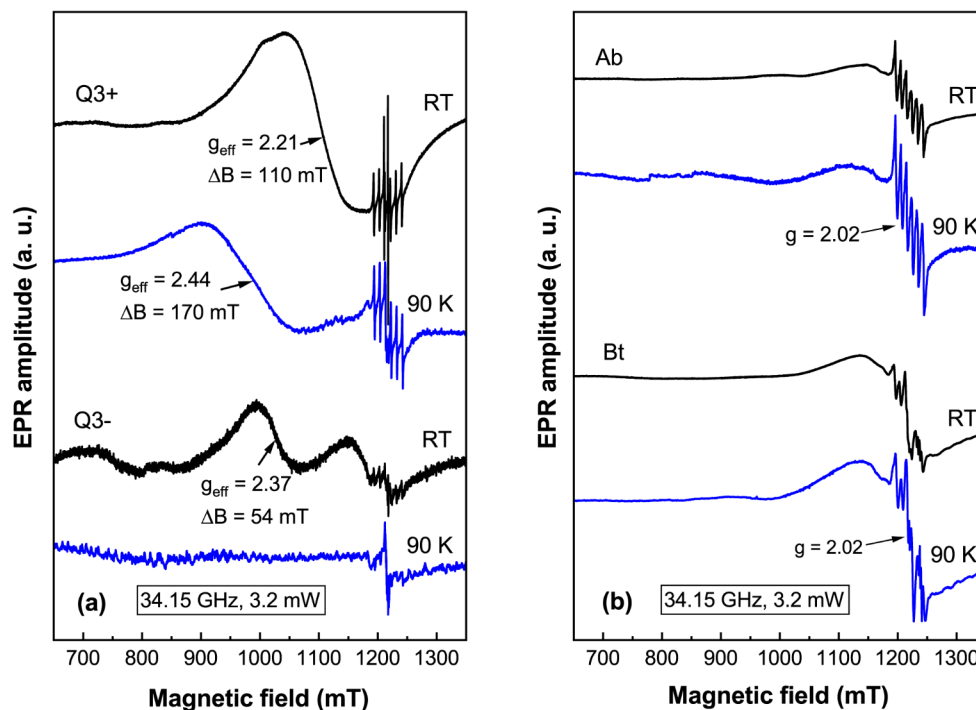
Fig. 3 Q-band EPR spectra measured at RT (black) and 90 K (blue) on the Q3 + and Q3- quartz (**a**) and associated mineral Ab and Bt (**b**) samples

mT did not exhibit any significant changes in the position or linewidth at low temperature (Fig. 3b).

The isolated Mn^{2+} spectra of the quartz samples are detailed in Fig. 4a. Two Mn^{2+} centers were observed, namely Mn(I), present in all samples, and Mn(II), present in Q1+, Q1- and Q3-. The simulated spectra of the two centers, obtained with the parameters from Table 1, are superimposed onto the experimental spectrum of each quartz sample. Based on the EPR spectra intensity, the Mn^{2+} concentration is of the order of 10^{-2} at% in the Q1 and Q3 samples, and up to an order of magnitude higher in the Q2 samples. The Mn^{2+} spectra of the associated mineral samples are displayed in Fig. 4c. In the case of the Ab sample, the experimental Mn^{2+} spectrum was reasonably well simulated with the Mn(Ab) spectrum calculated with the following parameters: $g = 2.0011 \pm 0.0002$, $A = 9.42 \pm 0.02$ mT, $D = 35.0 \pm 2.0$ mT, $E = 10.0 \pm 1.0$ mT. The simulation (sim.) of the experimental Ab spectrum improved when the Mn(II) spectrum was added to the Mn(Ab) spectrum.

The narrow lines positioned close to the center of the Mn^{2+} spectra belong to E_1' centers with rhombic symmetry, associated with oxygen vacancies (Mashkovtsev and Pan 2013). Figure 4b displays the spectra of these centers in the six quartz samples, recorded at 3 μW microwave power with 50 accumulated scans because of their strong saturation properties. The g-factor values of the E_1' centers, used in the simulation of the experimental spectra, varied slightly from sample to sample. The values listed in Table 1 are average g-values, the error margins covering all the values determined for the six samples. These values are comparable

with those reported for the E_1' centers in synthetic quartz measured in the X-band (Jani et al. 1983) and in natural quartz measured in the W-band (93 GHz) (Poolton et al. 2000). The differences between the experimental and simulated spectra in Fig. 4b could be due to the presence of more than one type of E' centers in each quartz sample and/or the presence of another defect with an EPR line overlapping the E_1' spectrum.

The EPR spectra of the quartz samples recorded at 90 K evidence the emergence of an intense twelve lines structure around 1220 mT and a weaker structure of six lines around 1185 mT (Fig. 5a). As shown in Fig. 5b, they can be explained by the anisotropic hyperfine interaction with an ^{27}Al nucleus (I = 5/2) and are characteristic to the $[AlO_4]^0$ centers, also called Al-h, consisting of substitutional Al^{3+} ions at Si^{4+} sites, with charge compensation at distance. The EPR parameters used in the simulation of the experimental spectra of the six samples also varied slightly from sample to sample. The average values of the EPR parameters of the $[AlO_4]^0$ centers are listed in Table 1, with the error margins covering all the values determined for the six samples. The determined values are comparable with those reported for the $[AlO_4]^0$ centers in other samples of natural quartz (Poolton et al. 2000; Kabacinska and Timar-Gabor 2022).

To verify how the heat sensitivity of the colored Albeşti quartz (Pantia and Filiuţă 2021) was reflected in the EPR spectra, the quartz samples were subjected to isochronal annealing at successive temperatures in 100°C steps up to 500°C. After a 30 min. annealing at a set temperature, the samples were cooled down to RT and measured.

Fig. 4 Q-band EPR spectra measured at room temperature (RT) (solid black) on the six quartz samples at (**a**) 0.78 mW and (**b**) 0.003 mW microwave power and the calculated Mn^{2+} (**a**) and E_1' centers spectra (**b**) (dot/dash lines); (**c**) Q-band EPR spectra of the Ab and Bt associated minerals (solid black) together with the simulated Ab spectrum (dash red), calculated as the sum of the simulated Mn(Ab) (dot green) and Mn(II) (dot blue) spectra
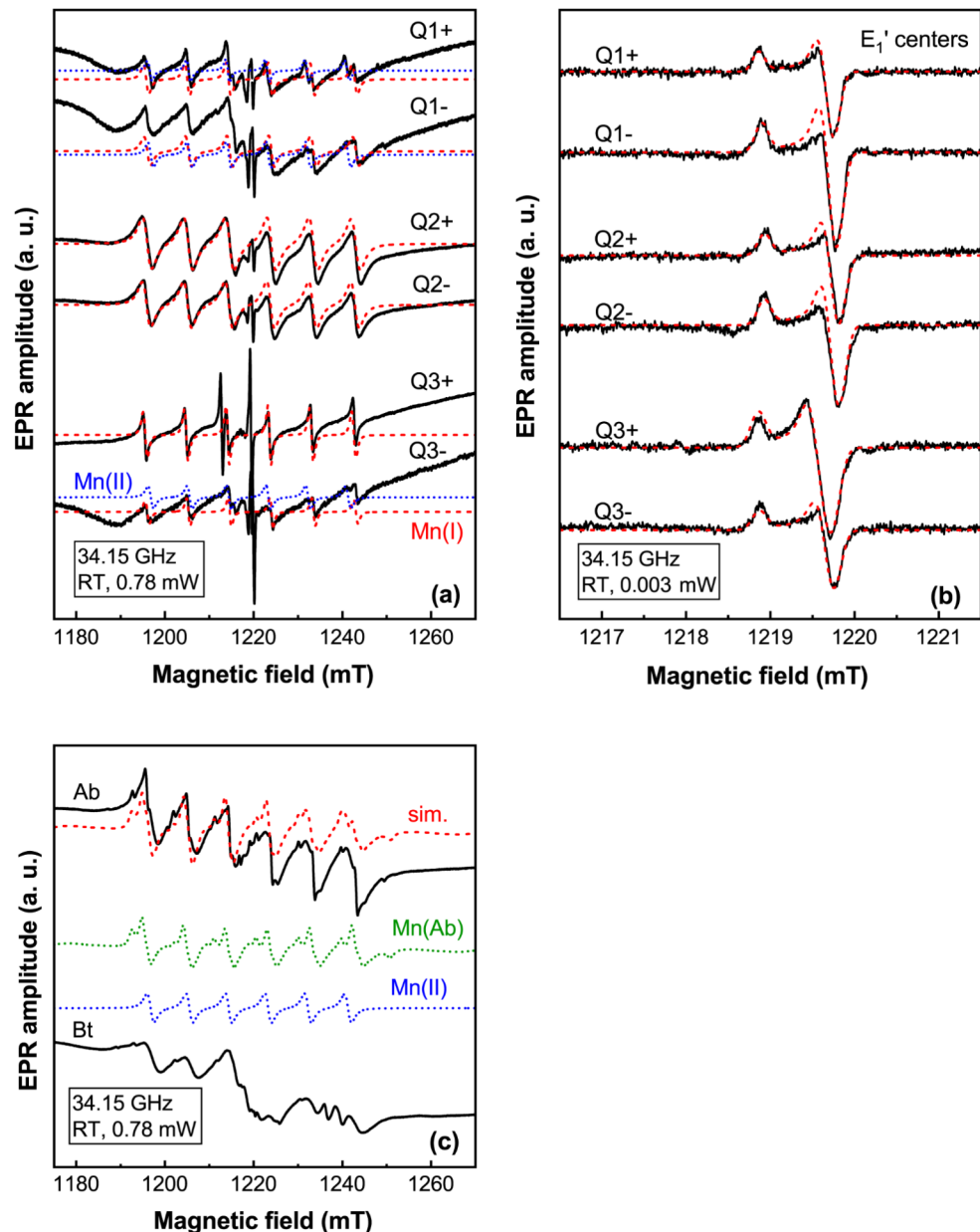
The associated mineral samples were also subjected to an annealing treatment of 30 min. at 500°C, for comparison. Figure 6a displays the EPR spectra of the quartz and associated mineral samples after the annealing treatment at 500°C.

Significant evolutions/transformations of the paramagnetic centers can be observed. After the final treatment at 500°C the E_1' and $[AlO_4]^0$ spectra disappear, the Mn^{2+} spectrum diminishes considerably and a broad line appears in the same spectral region. For all quartz samples another broad line appears at $g_{eff} \sim 2.38$ (Fig. 6a, b), that is not found in the spectra of the annealed associated minerals.

In the case of the associated mineral samples, the Mn^{2+} spectrum also diminishes (Ab) or completely disappears (Bt) after annealing at 500°C. A broad line appears in the

spectra of both annealed samples at $g_{eff} \sim 2.21$, probably due to the formation of an iron rich magnetic phase (Chang et al. 2012).

Figure 6c details the annealing induced changes in the spectrum of the blue quartz Q1 + sample, which are the same for all quartz samples. The comparison of the EPR spectra recorded at RT before annealing and after the 300°C and 500°C annealing steps shows that the E_1' lines increased in intensity after annealing at 300°C and disappeared at 500°C. The E_1' spectrum measured after the 300°C annealing step is displayed in Fig. 6d, together with the simulated spectrum with the g-values from Table 1. The $[AlO_4]^0$ lines completely vanished in the spectrum recorded at 90 K after the 500°C annealing step (Fig. 6c), while an isotropic line

Table 1 EPR parameters of the paramagnetic centers observed in the quartz samples

Center	Sample / microwave band	T (K)	g_x, g_y, g_z	A_x, A_y, A_z (mT)	Q_x, Q_y, Q_z (mT)	Reference
Mn(I)	All Q-band	RT	2.0011 ± 0.0001	9.42 ± 0.02	-	This work, Rao et al. (1989)
Mn(II)	Q1+, Q1-, Q3- Q-band	RT	2.0018 ± 0.0002	8.90 ± 0.05		This work
E_1'	All Q-band	RT	2.00035 ± 0.00005 2.00058 ± 0.00005 2.00184 ± 0.00005	-	-	This work
E_1'	Synthetic quartz X-band	RT	2.00029 2.00049 2.00176	-	-	Jani et al. (1983)
E_1'	Natural quartz W-band	RT	2.00032 2.00051 2.00181	-	-	Poolton et al. (2000)
$[AlO_4]^0$	All Q-band	90	2.0607 ± 0.0001 2.0084 ± 0.0001 2.0017 ± 0.0001	0.48 ± 0.05 0.61 ± 0.04 0.60 ± 0.02	-0.022 -0.015 0.037	This work
$[AlO_4]^0$	natural quartz W-band	15	2.0597 2.0082 2.0018	-	-	Poolton et al. (2000)
$[AlO_4]^0$	Natural quartz X-band	90	2.0603 2.0083 2.0021	0.499 0.606 0.649	-0.022 -0.015 0.037	Kabacinska and Timar-Gabor (2022)

Note The Q-values of the Al nucleus were taken from Mashkovtsev and Pan (2013) and the g and A axes were taken as coincident for convenience

Fig. 5 (**a**) Q-band EPR spectra measured at 90 K on the six quartz (black) and associated mineral Ab (red) and Bt (blue) samples. (**b**) Experimental (black) and calculated (red) spectra of the $[AlO_4]^0$ centers in the six quartz samples
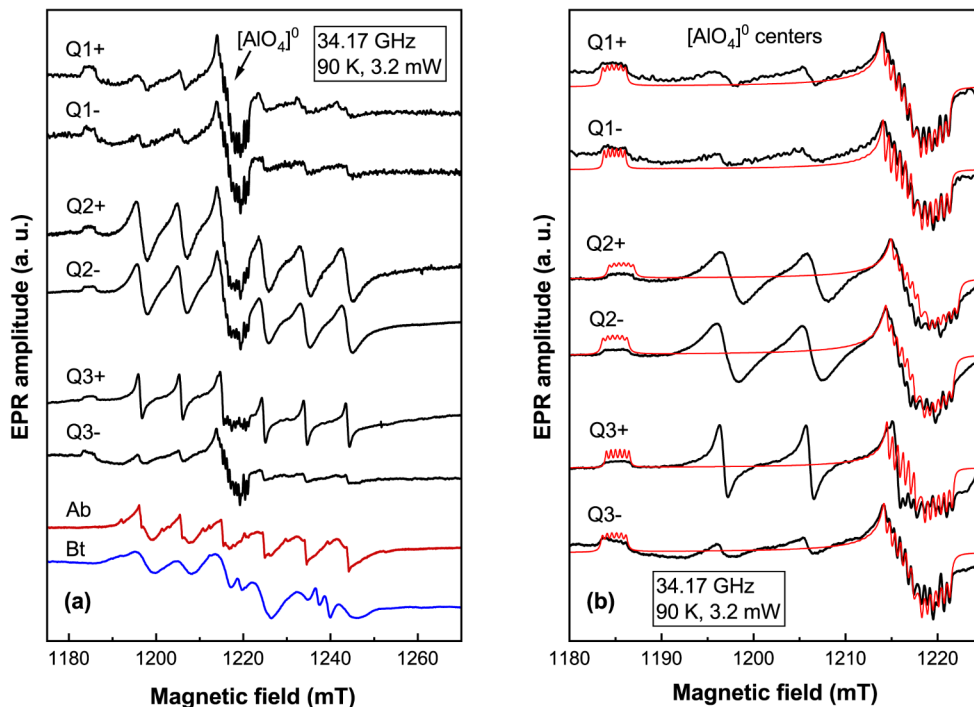

with g = 2.00266 and ΔB = 0.52 mT linewidth emerged, similar to the X1 signal observed by Poolton et al. (2000) and tentatively attributed to a carbon free radical.

The evolution of the E_1' centers concentration in all the quartz samples with the annealing temperature is presented in Fig. 7. The amplitudes of the recorded E_1' spectra were normalized with respect to the highest value, reached in all cases after annealing at 300°C. For all samples, the E_1' spectrum/concentration reached the maximum value at 300°C and then dropped sharply at 400°C, vanishing completely at 500°C.

Fig. 6 Q-band EPR spectra measured at (**a**) RT on the six quartz (black) and associated mineral Ab (red) and Bt (blue) samples subjected to 30 min. annealing at 500°C; (**b**) RT on the blue Q1 + quartz, Ab and Bt samples, pristine (black) and after a 30 min. annealing treatment in air at 500°C (red); (**c**) RT and 90 K on the Q1 + quartz sample, pristine (black) and after 30 min. annealing at the specified temperatures. (**d**) Experimental (black) and calculated (red) EPR spectra of the E_1' in the Q1 + quartz sample after 30 min. annealing at 300°C
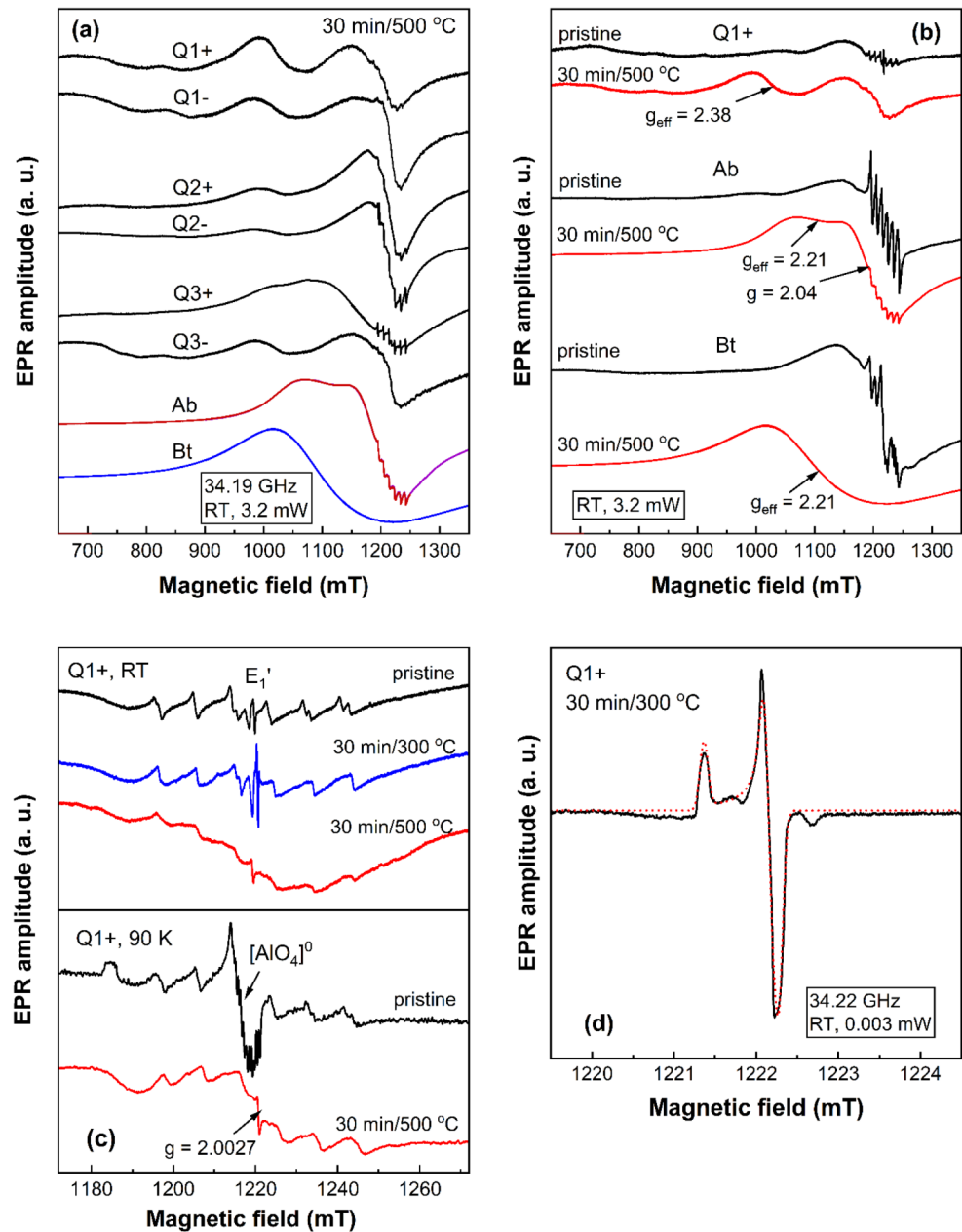
This behavior is similar with the one reported for the E_1' centers artificially produced by irradiation in synthetic quartz, which become annealed out between 300 and 450°C (Jani et al. 1983). However, unlike the present case, the E_1' centers in the natural quartz reported in ref. (Poolton et al. 2000) were not affected by annealing up to 500°C.

Discussion

The results of the EPR investigations show that the Albești quartz contains relatively low amounts of paramagnetic centers, with only two impurities, Mn and Al, clearly identified.

While the Al^{3+} ions substitute Si in the quartz lattice, forming the $[AlO_4]^0$ centers, the localization of the Mn^{2+} ions is not as straightforward.

The spectrum of the Mn(I) centers, consisting of the six hyperfine lines (I = 5/2) of the central electronic transition $M_S = 1/2 \leftrightarrow M_S = -1/2$ of the Mn^{2+} ions, was previously observed in natural quartz and in its surrounding carbon based mantle (Rao et al. 1989) and attributed to sixfold oxygen coordinated Mn^{2+} ions in a highly disordered environment. A plausible localization of the Mn^{2+} ions would be in a disordered/amorphous phase, at quartz grain boundaries or fissure planes. The presence of a disordered minority phase is supported by the EPR spectra from Fig. 2. Thus, the
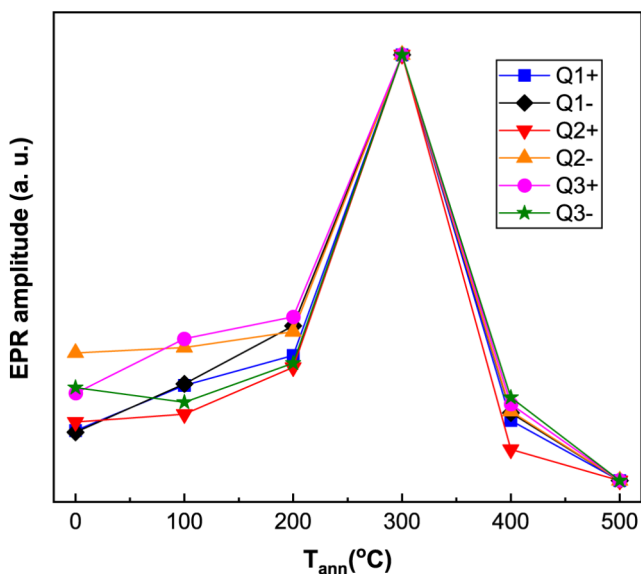
Fig. 7 The relative variation of the EPR spectrum amplitude of the E_1' centers with the annealing temperature for the six quartz samples, normalized to the maximum value at 300 °C

Q-band Mn(I) spectrum is the most intense for the Q2 + and Q2- samples (Fig. 2a), which also exhibit weak Fe^{3+} lines in their X-band spectra (Fig. 2b), assumed to belong to traces of associated minerals. Moreover, the Mn(I) and Mn(Ab) centers have similar hyperfine A and g-parameter values, showing that they could consist of Mn^{2+} ions localized in the disordered and crystalline phases, respectively, of the same mineral. This mineral could be either albite or muscovite, according to the X-ray diffraction pattern of the Ab sample (Fig. S1c). The spectrum of the Mn(II) centers is also typical for Mn^{2+} ions in a disordered environment. A comparison of the calculated Mn(II) spectrum with the experimental Ab and Bt spectra shows that the Mn(II) centers could be present in both associated mineral samples (Fig. 4c, S2). In fact, the Ab spectrum is better simulated by a sum of the Mn(Ab) and Mn(II) spectra.

Previous EPR investigations of albite (Larikov et al. 2023 and the references cited therein), plagioclase (Larikov et al. 2023; Scala et al. 1978) and muscovite (Muller and Calas 1993; Tiwari et al. 2015), of various origins, reported Mn^{2+} spectra characteristic to disordered environments, with a wide range of g-values and hyperfine parameters that could differ as much as 0.4 mT for the same type of mineral. In the case of the albite and plagioclase, the proposed localization of the Mn^{2+} ions was in minority phases along grain boundaries (Larikov et al. 2023), in twin boundary regions or into regions of structural transformation (Scala et al. 1978). The information gained from literature is thus too scarce to permit a clear assignment of the Mn(I), Mn(Ab) and Mn(II) centers to a specific associated mineral. Nevertheless, based on our results we can conclude that the Mn^{2+} ions observed

by Rao et al. (1989) and in the present study are not bound in the quartz lattice.

The low concentration (less than 1–2 wt%) and high disorder degree of the minority phases in the quartz samples would explain why they are not visible in the X-ray diffraction pattern of the Q2 quartz (Fig. S1a). Such phases can often be detected and even identified by EPR spectroscopy due to its high sensitivity (Nistor et al. 2013; Mihalcea et al. 2024), although they are below the detection limit of XRD.

One of the limitations of the conventional X- and Q-band EPR is that it can mainly detect the paramagnetic centers with half-integer electron spins. Thus, besides the observed Mn^{2+} and Al^{3+} related centers, other so-called "EPR silent" impurities, with integer electron spins and large zero field splittings (e.g. Fe^{2+}, Mn^{3+}), observable only at higher microwave frequencies and magnetic fields, could be present as well. Trace amounts of iron (below 0.1 wt%) and titanium (0.005–0.01 wt%) have been detected in the quartz samples by electron microprobe investigations (unpublished). As the EPR spectra do not exhibit the lines characteristic to the Fe^{3+} centers in quartz (Mashkovtsev and Pan 2013), it is possible that the detected iron is present as Fe^{2+}, either isolated or in minority iron rich phases, such as ilmenite. The detected titanium could be present as diamagnetic Ti^{4+} in phases such as ilmenite or rutile (Pantia and Filiuţă 2021). One way to make these impurities detectable by EPR is to change their electronic state by submitting the sample to annealing treatments that could induce either the recombination of some defect centers, with the generation of charge carriers that could become trapped at the respective impurities, or the decomposition of some compounds into new EPR detectable phases (Nistor et al. 2013, 2014; Mihalcea et al. 2024).

The isochronal annealing treatments of our quartz samples induced indeed significant changes in the EPR spectra, which can be explained by these mechanisms. Thus, the spectra of all the quartz samples exhibited, after annealing at 500 ºC, a broad line with $g_{eff} \sim 2.38$ (Fig. 6a, b), that was not present in the spectra of the annealed associated minerals. This line could be due to the formation of magnetic clusters of iron oxides, such as hematite or magnetite (Chang et al. 2012; Allieta et al. 2020), most likely at fissure planes or grain boundaries. This would also explain the rusty coloration observed for some of the quartz grains after heating at 500°C (Pantia and Filiuţă 2021). The observed decrease in the isolated Mn^{2+} ions spectrum intensity could be caused by either a thermally induced aggregation process, leading to a broadening of the EPR lines due to the increased dipolar magnetic interaction, or a change of the Mn^{2+} oxidation state to Mn^{3+}. The increase in the E1' centers concentration up to 300°C was correlated with the decay of the $[AlO_4]^0$ centers and the thermal release of holes (Jani et al. 1983).

A comparison of the EPR spectra of the six samples, measured before and after the annealing treatment, shows only two differences that separate the quartz samples by origin, rather than color. Thus, the Mn^{2+} concentration is higher in the Q2 samples, while the Q3 samples contain a small amount of magnetically ordered phase. We can conclude that there are no consistent differences in the EPR spectra of the six quartz samples associated with the blue coloration. According to our results, the coloration of the Albești quartz does not involve the presence of paramagnetic centers or minority magnetic phases, at least not ones detectable by conventional X- and Q-band EPR. Considering also the previously published optical information (Pantia and Filiuță 2021), it is quite possible that the responsible mechanism does not even take place at atomic level, but at a larger scale, involving spatial defects, defect aggregates and/or minority phase clusters. Further investigations of the Albești blue quartz by complementary techniques could help elucidate this issue.

Conclusions

The EPR signature of the blue quartz from the Albești granite was determined by an extensive multi-frequency (X- and Q-band) EPR study, carried out on three quartz samples with different levels of coloration (blue, pale blue and white) and their colorless counterparts collected from the same rocks, as well as associated feldspar and biotite samples, to account for possible contaminations. The evolution of the identified paramagnetic centers under isochronal annealing up to 500°C was also monitored, in order to observe possible correlations with the thermally induced loss of color of the heat sensitive Albești blue quartz.

As evidenced by the EPR studies, the quartz samples contain low amounts (less than 0.1 at%) of Mn^{2+} and Al^{3+} impurities. The Mn^{2+} concentration is significantly larger in the pale blue and the corresponding colorless quartz samples. While the Al^{3+} ions are localized substitutionally at Si sites in quartz, forming $[AlO_4]^0$ centers, the Mn^{2+} ions are most likely localized in amorphous traces of associated minerals, at grain boundaries or in fissure planes in quartz. Magnetic clusters have been observed in the pristine white sample and its colorless counterpart. The isochronal annealing up to 500°C induced the strong decrease of the isolated Mn^{2+} ions spectrum and the formation of a new magnetic phase in all quartz samples, assumed to consist of iron oxide clusters at quartz grain boundaries or fissure planes. A low concentration of E_1' centers was observed in all quartz samples, with a typical evolution under annealing, i.e. increase in concentration at ~300°C, followed by a strong decrease at 400°C and complete decay at 500°C. Their evolution is correlated with the evolution of the hole $[AlO_4]^0$ centers, as previously reported.

No consistent differences associated with the blue coloration were observed among the six quartz samples, before and after annealing. It is plausible that the mechanism responsible for the heat sensitive coloration of the Albești quartz does not involve paramagnetic centers, at least not ones detectable by conventional EPR, or does not even take place at atomic level, but at a larger scale, involving spatial defects, defect aggregates and/or minority phase inclusions.

References

Allieta M, Beranová K, Marelli M, Coduri M, Stefan M, Ghica D, Morello G, Malara F, Naldoni A (2020) Electron Small Polaron and magnetic interactions direct anisotropic growth of Silicon-Doped Hematite nanocrystals. Cryst Growth Des 20(7):4719–4730

Buhay WM, Schwarcz HP, Grün R (1988) ESR dating of fault gouge: the effect of grain size. Quat Sci Rev 7:515–522

Cerin D, Götze J, Pan Y (2017) Radiation-induced damage in Quartz at the Arrow Uranium Deposit, Southwestern Athabasca Basin, Saskatchewan. Canad Mineral 55:457–472

Chang L, Winklhofer M, Roberts AP, Dekkers MJ, Horng CS, Hu L, Chen Q (2012) Ferromagnetic resonance characterization of greigite (Fe_3S_4), monoclinic pyrrhotite (Fe_7S_8), and non-interacting titanomagnetite ($Fe_{3-x}Ti_xO_4$). Geochem Geophys Geosyst 13:Q05Z41

Ghica D, Stefan M, Ghica C, Stan GE (2014) Evaluation of the segregation of Paramagnetic Impurities at Grain Boundaries in Nanostructured ZnO films. ACS Appl Mater Interfaces 6:14231–14238

Götze J (2009) Chemistry, textures and physical properties of quartz – geological interpretation and technical application. Mineral Mag 73(4):645–671

Götze J, Pan Y, Müller A (2021) Mineralogy and mineral chemistry of quartz: a review. Mineral Mag 85:639–664

Iddings JP (1904) Quartz-feldspar-porphyry (graniphyro liparose-alaskose) from Llano, Texas. J Geol 12(3):225–231

Jani MG, Bossoli RB, Halliburton LE (1983) Further characterization of the E'$_1$ center in crystalline SiO_2. Phys Rev B 27:2285–2293

Kabacinska Z, Timar-Gabor A (2022) Dating sediments by EPR using Al-h centre: a comparison between the properties of Fine (4–11 μm) and coarse (> 63 μm) quartz grains. Molecules 27(9):2683

Kim D, Jin YH, Jeon KW, Kim S, Kim SJ, Han OH, Seo DK, Park JC (2015) Blue-silica by Eu^{2+}-activator occupied in interstitial sites. RSC Adv 5:74790–74801

Larikov AL, Zaiats O, Bagmut MM (2023) EPR characteristics of feldspars from granites of Ruska Polyana massif of

Korsun-Novomyrhorod pluton (Ukrainian Shield). Mineral J 45:50–58

Mashkovtsev RI, Pan Y (2013) Nature of paramagnetic defects in α-quartz: progresses in the first decade of the 21st century. In: Novak B, Marek P (eds) New developments in quartz research: varieties, crystal chemistry and uses in technology. Nova, New York, pp 65–104

Mihalcea CG, Stefan M, Ghica C, Florea OG, Stanoiu A, Simion CE, Somacescu S, Ghica D (2024) In-depth insight into the structural properties of nanoparticulate NiO for CO sensing. Appl Surf Sci 651:159252

Miyako Y, Date M (1964) Hyperfine fields of Mn^{2+} and Mn^{4+} ions in MgO. J Phys Soc Japan 19:784

Muller J-P, Calas G (1993) Mn^{2+}-bearing kaolinites from lateritic weathering profiles: geochemical significance. GCA 57:1029–1037

Nassau K (1983) The Physics and Chemistry of color: the fifteen causes of color, Wiley, New York, 454 p, ISBN 0-471-86776-4

Negulescu E (2013) Semnificaţia mineralelor şi a asociaţiilor minerale în determinarea istoriei metamorfice a cristalinului Masivului Leaota, Tehnopress, Iaşi, 100 p, ISBN 978-973-702-988-1

Nicolini KP, Lombardi KC, Schreiner WH, Mazzaro I, Wypych F, Mangrich AS (2009) Evidence of weathering stages of phyllosilicates from biotite/muscovite to kaolinite, probed by EPR spectroscopy. Min Petrol 97:139–144

Nistor SV, Ghica D, Stefan M, Nistor LC (2013) Sequential thermal decomposition of the shell of cubic ZnS/Zn(OH)2 core−shell quantum dots observed with Mn^{2+} probing ions. J Phys Chem C 117:22017–22028

Nistor SV, Stefan M, Ghica D (2014) Pulse annealing electron paramagnetic resonance with probing transition ions: application to thermal formation and growth of nanoZnO. J Therm Anal Calorim 118:1021–1031

Nistor SV, Stefan M, Nistor LC, Kuncser V, Ghica D, Vlaicu ID (2016) Aggregates of Mn^{2+} ions in mesoporous self-assembled cubic ZnS:Mn quantum dots: composition, localization, structure, and magnetic properties. J Phys Chem C 120:14454–14466

Pantia AI, Filiuţă AE (2021) Heat sensitive blue quartz – the unusual occurrence of Albeşti, Romania. Carpathian J Earth Environ Sci 16(1):175–186

Pelletier M (2016) The Rainy River Gold Deposit, Wabigoon Subprovince, western Ontario: style, timing and structural controls on ore distribution and grades. Thesis presented for the degree of Master of Science, Université du Québec, Centre Eau Terre Environnement, 368p

Perlson BD, Weil JA (2008) Electron paramagnetic resonance studies of the E' centers in alpha-quartz. Can J Phys 86:871–881

Poolton NRJ, Smith GM, Riedi PC, Bulur E, Bøtter-Jensen L, Murray AS, Adrian M (2000) Luminescence sensitivity changes in natural quartz induced by high temperature annealing: a high frequency EPR and OSL study. J Phys D Appl Phys 33:1007–1017

Preusser F, Chithambo ML, Gotte T, Martini M, Ramseyer K, Sendezera EJ, Susino GJ, Wintle AG (2009) Quartz as a natural luminescence dosimeter. Earth Sci Rev 97:184–214

Rao PS, Weil JA, Williams JAS (1989) EPR investigation of carbonaceous natural quartz single crystals. Can Mineral 27:219–224

Rossman GR (1994) Colored varieties of the silica minerals. In: Heaney PJ, Prewitt CT, Gibbs GV (eds) Silica: physical behavior, Geochemistry, and materials applications reviews in Mineralogy, vol 29. Mineralogical Society of America, Washington DC, pp 433–467

Scala CM, Hutton DR, McLaren AC (1978) NMR and EPR studies of the chemically intermediate plagioclase feldspars. Phys Chem Min 3:33–44

Seifert W, Rhede D, Förster HJ, Thomas R (2009) Accessory minerals as fingerprints for the thermal history and geochronology of the Caledonian Rumburk granite. Neues Jahrbuch für Mineralogie Abhandlungen 186(2):215–233

Seifert W, Thomas R, Rhede D, Förster HJ (2010) Origin of coexisting wüstite, Mg-Fe and REE phosphate minerals in graphite-bearing fluorapatite from the Rumburk granite. Eur J Mineral 22:495–507

Seifert W, Rhede D, Thomas R, Forster HJ, Lucaseen F, Dulski P, Wirth R (2011) Distinctive properties of rock-forming blue quartz: inferences from a multi-analytical study of submicron mineral inclusions. Mineral Mag 75(4):2519–2534

Stoll S, Schweiger A (2006) EasySpin, a comprehensive software package for spectral simulation and analysis in EPR. J Magn Reson 178:42–55

Tiwari A, Tripathi A, Pathak AP (2015) Swift heavy ion irradiation of muscovite and biotite substrates. Nucl Instrum Meth B 343:9–14

Zolensky ME, Sylvester PJ, Paces JB (1988) Origin and significance of blue coloration in quartz from Llano rhyolite (llanite), north-central Llano County, Texas. Am Min 73:313–323